chemosensors

MDPI

Review

Atomistic Descriptions of Gas-Surface Interactions on Tin Dioxide

Stefan Kucharski and Chris Blackman *

Department of Chemistry, University College London, 20 Gordon Street, London WC1H 0AJ, UK; stefan.kucharski.13@ucl.ac.uk

* Correspondence: c.blackman@ucl.ac.uk; Tel.: +44-208-7679-4703; Fax: +44-208-7679-7463

Abstract: Historically, in gas sensing literature, the focus on "mechanisms" has been on oxygen species chemisorbed (ionosorbed) from the ambient atmosphere, but what these species actually represent and the location of the adsorption site on the surface of the solid are typically not well described. Recent advances in computational modelling and experimental surface science provide insights on the likely mechanism by which oxygen and other species interact with the surface of SnO_2, providing insight into future directions for materials design and optimisation. This article reviews the proposed models of adsorption and reaction of oxygen on SnO_2, including a summary of conventional evidence for oxygen ionosorption and recent operando spectroscopy studies of the atomistic interactions on the surface. The analysis is extended to include common target and interfering reducing gases, such as CO and H_2, cross-interactions with H_2O vapour, and NO_2 as an example of an oxidising gas. We emphasise the importance of the surface oxygen vacancies as both the preferred adsorption site of many gases and in the self-doping mechanism of SnO_2.

Keywords: SnO_2; sensor; mechanism; operando; spectroscopy; adsorbates; vacancies

Citation: Kucharski, S.; Blackman, C. Atomistic Descriptions of Gas-Surface Interactions on Tin Dioxide. *Chemosensors* **2021**, *9*, 270. https://doi.org/10.3390/chemosensors9090270

Academic Editors: Valerio Vignoli and Enza Panzardi

Received: 27 July 2021
Accepted: 2 September 2021
Published: 18 September 2021

1. Introduction

Conductometric gas sensors (CGS) are small, easily fabricated devices that require relatively low power consumption and contain no moving parts. In their simplest form, they consist only of two electrodes interconnected by a layer of gas-sensitive material and can be printed as films directly onto a substrate [1,2]. These characteristics make CGS perfect for mass-scale production and portable device applications. Large scale deployment of such devices could, for example, screen for diabetes or detect imminent electric transformer failure by detecting gases characteristic to the processes [3,4]. However, despite their many advantages, CGS often suffer from cross-sensitivity to interfering gases and performance deterioration over time [5,6], and the main driving force in CGS research targets improvements in sensors' sensitivity, selectivity and response time. Insufficient understanding of the mechanisms of surface reactions makes improvements possible only through empirical exploration.

Spectroscopic investigation of sensors under working conditions is often unattainable due to the UHV requirement of many analytical techniques, for example, X-ray photoelectron spectroscopy (XPS), ion scattering spectroscopy (ISS) or low-energy electron diffraction (LEED). In the catalytic community, this incompatibility is known as the "pressure gap"; this is why early sensor operation models were developed by applying prevailing chemistry principles to explain phenomenological observations. The most prevalent model is the oxygen ionosorption mechanism, which explains the sensor's increased resistance on exposure to oxygen through dissociative adsorption of ambient dioxygen to form ions electrostatically stabilised by the surface [7–13].

It was conjectured that because of its electron affinity, oxygen would withdraw electrons from the conduction band of an n-type semiconductor, and "consequently, there will be no chemisorbed oxygen atoms, but oxygen ions, in the surface" [14]. In this description,

the localisation of negative charge at the surface of SnO_2 grains results in a charge depletion zone below the surface, which constitutes a potential barrier for electrons trying to cross the grain boundary, effectively increasing the sensor's resistance. Usually, the process is only broadly described using the following reaction equation [7,8], which sometimes is extended to include intermediate O_2 physisorbed and O_2^- chemisorbed species [10,15].

$$\frac{1}{2}\,O2(gas) + e^- \rightarrow O^-$$

$$O2(gas) \rightarrow O2(phys) + e^- \rightarrow O2^- + e^- \rightarrow 2\,O^-$$

The lack of reference to adsorption sites is not the only problem with ionosorption models, however, which also do not consider whether the oxygen dissociation is symmetric, and if asymmetric, the fate of the other oxygen atom. Moreover, the models often assume that there is no mass transport between the bulk of the sensor and the gas phase [7,10,12], which is not a valid assumption to make, as explained further below. Finally, there is also the question of the existence of O^- ions adsorbed at the surface, for which there is no conclusive evidence after decades of research [16].

In the absence of adequate analytical techniques, early atomistic insight into the surface processes of gas sensing was provided by computational studies. The chemical state of the surface can be analysed either kinetically, modelling the temporal evolution of a system defined by a set of chemical reactions by optimising an array of parameters, or thermodynamically, estimating the most stable adsorption configurations from first-principles calculations on a model surface, such as a cluster or a slab. The former approach may be used to, for example, estimate the equilibrium density of oxygen adsorbates on O_2 or predict sensor behaviour in varying oxygen pressure [7,15]. The latter is essential in discovering possible adsorbate species and investigating their effects on the surface [17,18]. However, analysis of sensors working under conditions close to ambient has become increasingly more available with the advent of operando spectroscopy. It offers microscopic insight into processes formerly studied only post-mortem in UHV after exposure to a target gas in a preparation chamber, thus presenting new possibilities. For example, changes in the electronic structure of a working sensor may be studied under dynamic pressure and temperature conditions through Near Ambient Pressure (NAP) XPS with simultaneous resistance measurements [19].

In this work, the authors attempt to summarise the proposed mechanisms for the interactions of SnO_2 with oxygen and reducing and oxidising gases as understood from phenomenological and computational studies and highlight those supported by spectroscopic evidence. Since providing an atomistic description of such interactions is the aim of this review, a sensible place to start is by considering the atoms of the surface itself, which is the subject of the next section.

2. The Dynamic Surfaces of Tin Dioxide

Tin dioxide, SnO_2, is among the most common sensitive materials used in CGS. It is abundant, inexpensive, non-toxic and shows excellent stability to reducing conditions. Since Taguchi introduced the first commercial SnO_2-based gas sensors in 1972, and this oxide has been the most widely studied gas-sensitive material, with an initial focus on detecting reducing gases such as CO and volatile organic compounds (VOC). However, recently the focus is shifting towards low-temperature NO_2 detection.

The crystalline form of SnO_2, known as cassiterite, is a rutile-type tetragonal structure with lattice parameters a = b = 4.737 Å and c = 3.186 Å [20]. It is an intrinsic n-type semiconductor with a wide, direct bandgap of 3.6 eV [21], which also makes it transparent and of high interest in touchscreen electronics. Although the exact origin of the intrinsic conductivity is still debated, oxygen vacancies (V_O) seem to play an important role [22–25]; therefore, a change in the density of V_O will affect the sensor's resistance.

The surface is the interface of oxygen exchange between the bulk and the ambient and a terminal for interaction with other gases and thus requires due consideration.

Large SnO_2 single crystals, which are notoriously challenging to grow, preferentially expose the (110), (101) and (100) surfaces [26]. Of these three, the (110) was shown to have the lowest energy and is the subject of most computational adsorption studies [17,18,27–31], though some results are also available for the (101) surface [32,33]. Both surfaces feature bridging oxygen sites (O_{br}), which protrude outwards from the surface determined by the plane of Sn atoms. The (110) surface has another type of exposed oxygen atom, the in-plane oxygen (O_{pl}), which does not have a counterpart on the (101) surface, though the second layer (101) oxygen atoms (first subsurface oxygen) are sometimes referred to in that way.

O_{br} atoms can be removed to form vacancies in the process of surface reduction, facilitated by the dual valency of $Sn^{2+/4+}$. The removal results in either a partially or fully reduced surface, the latter indicating one with all O_{br} removed, as presented in Figure 1. The surface vacancies can migrate via in-plane sites into the bulk in a thermally activated process, which becomes noticeable at temperatures above 250 °C [24]. Moreover, the formation energies of these vacancies mutually depend on the defects' densities, as indicated by computational studies [34]. It means that while the initial reduction of the stoichiometric surface will proceed by mainly removing O_{br}, at a relative V_{br} density of 0.5, the formation energy difference between bridging and in-plane defects is much smaller, so both should coexist at the surface. Therefore, the equilibrium density of surface vacancies should depend not only on the chemical potential of gaseous oxygen but also on the density of subsurface V_O in bulk SnO_2, assuming the temperature is high enough for the atoms to reach their equilibrium position. The role of vacancies in sensor operation mechanisms is two-fold; as a self-doping mechanism, which provides intrinsic conductivity in SnO_2, and as the preferred adsorption site for oxygen, which does not adsorb onto stoichiometric surfaces of SnO_2, as indicated by many computational studies [17,28,32] and explained in the following section.

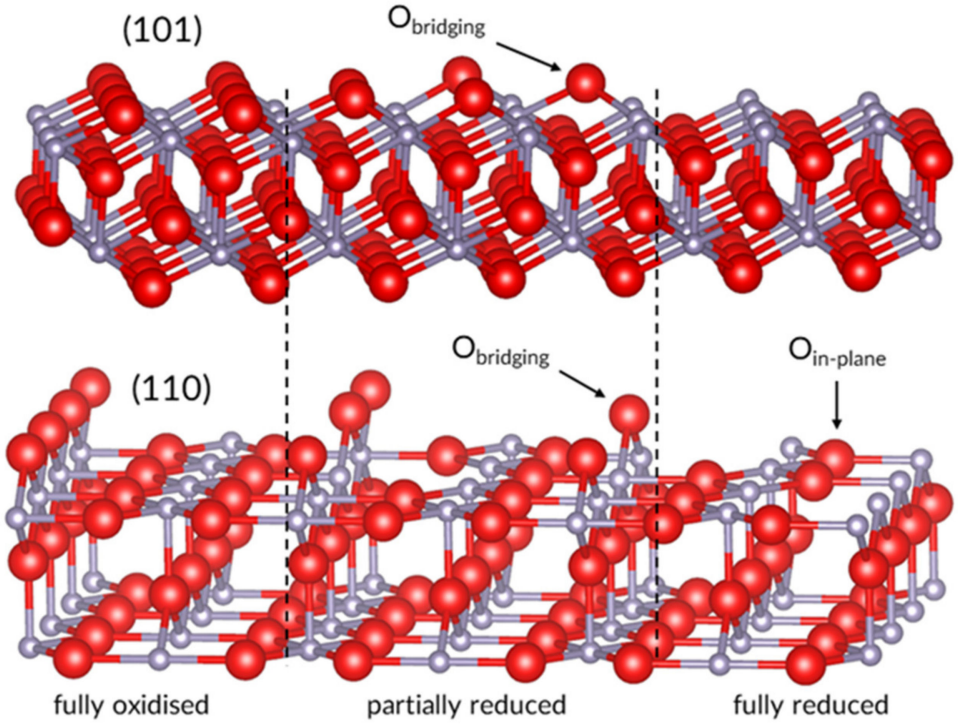

Figure 1. Progressing reduction of the (**110**,**101**) surfaces of SnO_2. Image prepared in VESTA [35].

3. Interactions with Oxygen

3.1. Insight from Computational Studies

The early computational work by Yamaguchi et al. on the surfaces of SnO_2 explored the adsorption energies of oxygen adsorbates placed on a (110) surface bridging vacancy us-

ing a point charge model [36]. They found that adsorbate interaction with a vacancy yields negative adsorption energies for a range of both mono- and diatomic species. According to their results, a molecule of oxygen can adsorb both in side-on and end-on configurations and can be singly or doubly charged, i.e., O_2^- and O_2^{2-}. The study also shows that an O^- adsorbate is stabilised by the surface vacancy with an energy similar to that of typical bridging lattice oxygen, O^{2-} (16.22 vs. 16.97 eV per $2O^-$). However, the authors acknowledge that the investigated configurations of oxygen adsorbates were guessed due to the lack of information on adsorption geometry.

In a follow-up letter, Yamaguchi considers the dissociation of oxygen on a fully reduced surface and concludes that the dissociation of O_2^{2-} leads to the formation of O^- monoatomic species, which are coupled with a V_{br} and immobilised by a rather sizeable potential barrier, and that this adsorption site is more favourable than a neighbouring Sn_{5c} site [27]. However, a more recent computational study suggests that the range of possible adsorbates is less diverse. Investigation of a similarly reduced surface led to the conclusion that the dissociation of O_2^{2-} results in the healing of two vacancies, i.e., the formation of O^{2-} ions indistinguishable from O_{br} [17]. The same study considers the adsorption of O_2 onto an isolated V_{br}, in which case they find that the dissociation of O_2 leads to the healing of the vacancy by one of the atoms, while the other becomes an O^- ion adsorbed onto a neighbouring Sn_{5c} site, as there are no other nearby vacancies to interact within the model. Therefore, it seems that O^- should only exist under particular circumstances as a remnant of the final steps of surface oxidation after nearly all vacancies have been healed. For both the reduced surface and an isolated vacancy, the dissociation has a relatively large activation energy (1.32 and 0.54 eV, respectively) [17], which is at variance with the results of Yamaguchi, who reports an activation barrier of only 0.09 eV [27]. Such a small barrier is unlikely as, experimentally, oxidation of the surface was determined to be a thermally activated process [37].

Prior to the dissociation, the molecular oxygen adsorbates may exist in a physisorbed state, where there is no charge transfer between the surface and the molecule, and in a chemisorbed state, where the molecule withdraws electron density from the surface. Currently, there is no agreement on whether the charge of the adsorbate is related to the adsorption geometry. While one DFT study finds that end-on and side-on configurations (Figure 2) correspond to superoxide and peroxide species, respectively [17], a different study only reports a side-on configuration for diatomic oxygen, which they assign to a superoxide [28]. In both studies, the adsorbate is bound to the V_{br} on one side and Sn_{5c} on the other, which seems to be the most favourable adsorption geometry; see O-lie in Figure 2.

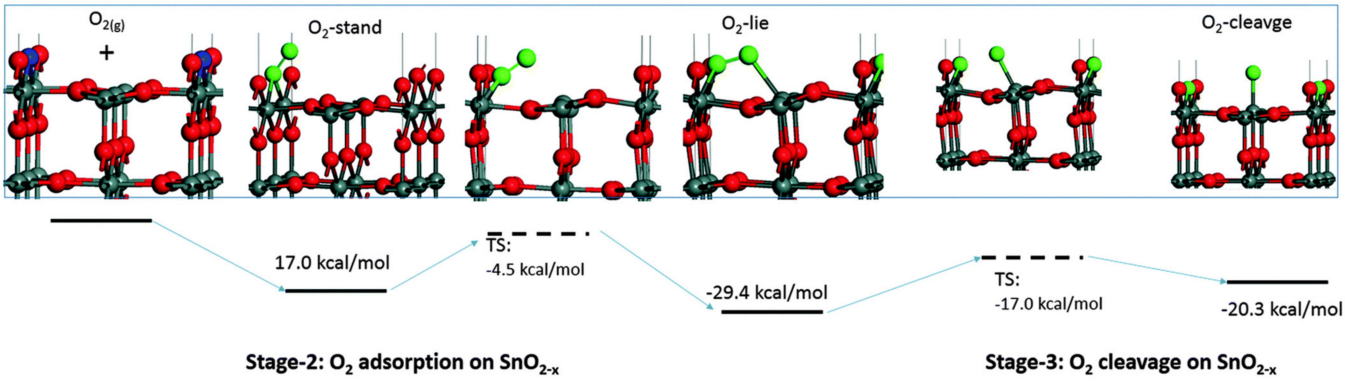

Figure 2. Adsorption of O_2 onto a (110) surface of SnO_2 with an isolated vacancy. From left: a (110) surface with a single (periodic) bridging vacancy (blue), "O-stand" superoxide molecular adsorbate in the end-on configuration, "O-lie" peroxide molecular adsorbate in the side-on configuration and "O-cleavage" monoatomic O^- adsorbate adjacent to a healed vacancy—now O_{br}. Reproduced with permission from Reference [17].

The above descriptions were of the (110) surface, for which most computational studies are performed, and there are limited data on the adsorption of O_2 onto other surfaces. An investigation of the (101) surface indicates that O_2 interaction mechanisms are similar to those of the (110) surface [32]. Only weak interactions are found for a stoichiometric surface, and the vacancy is again an essential active site. Upon adsorption onto an isolated vacancy on a partially reduced surface, the molecule transforms into a peroxide-like species with an adsorption energy of 1.02 eV. Unlike for the (110) surface, this adsorption configuration should not lead to dissociation into O^-, as the peroxide bond cannot break [32]. However, the adsorption of O_2 onto two neighbouring vacancies leads to the adsorbate dissociation and healing of both defects, similar to the (110) surface.

Although the localisation of electrons in the antibonding π^* orbitals of the peroxide adsorbates results in the formation of negatively charged species, this process should not lead to the accumulation of negative charge at the surface or a subsurface depletion layer. It was found that upon adsorption onto a vacancy, the oxidation state of a neighbouring Sn is changed from +2 to +4 [32]; therefore, the charge of the V_{br} should be -2 rather than 0 for the surface to remain overall charge-neutral. Because of this, the peroxide species should not contribute to a dipole layer formation, rather than to the localisation of electrons on the vacancy site.

Recently, a different computational description of the adsorption of O_2 onto SnO_2 was proposed, where instead of creating a vacancy, the surface was enriched with extra electrons to enable adsorption. The study shows that an electron added to the system can stabilise it by lowering the energy of one antibonding π^* orbital of $O_2{}^-$ to just above the valence band maximum [38]. In such a configuration, the molecule is bound to two neighbouring Sn_{5c} sites, and the negative charge of the adsorbate is not compensated by its location, as it lies outside of regular lattice anion sites. Therefore, this process should lead to the accumulation of charge at the surface. However, it is not entirely clear where the electrons come from in a system without oxygen vacancies or dopants, which could significantly alter the results by affecting the electronic structure of the surface [39]. The study also shows that introducing a second electron does not significantly affect the geometry of the adsorbate or the energy of the second π^* orbital. Instead, the second and subsequent electrons occupy the conduction band; therefore, the authors concluded that $O_2{}^{2-}$ should not form on the (110), (100) and (101) surfaces of SnO_2 [38]. This conclusion is at variance with the experimental evidence of peroxide $O_2{}^{2-}$ adsorbate [40], discussed in the following section.

The same study revisits the possibility of monoatomic oxygen adsorbates, pointed out by the authors as the species responsible for the observed resistance change [38]. Several adsorption configurations were found on the surface, which may be divided into two categories, "peroxide-like" and "lattice-like" species. The former is characterised by a peroxide bond to an O_{br} in addition to a bond to Sn_{5c}; this adsorption configuration is equivalent to the adsorption of $O_2{}^{2-}$ onto a V_{br}, and the authors conclude that it is charge neutral with respect to the lattice and should not affect the resistance of the sensor. The latter is bound to either one or two different Sn_{5c} sites in a geometry not far removed from the local coordination of lattice oxygen atoms; in this case, stable adsorption configurations were found only on the (100) surface, which features a considerable distortion of the adsorption site. On the (110) and (101) surfaces, all monoatomic adsorbates were found unstable to transformation into O_2 and $O_2{}^-$. Based on these results, the authors concluded that the resistance of SnO_2 is defined by interactions of O_2 with only the (100) surface. However, gas-sensitive phenomena were also observed on other surfaces, for example, an epitaxial (101) thin film [41], which shows that these results might be incomplete.

3.2. What Species Were Observed Spectroscopically?

Because of the aforementioned "pressure gap", the choice of analytical techniques suitable for studying gas sensors is limited, so the evidence is scarce. The most widely accepted evidence of oxygen ionosorption on SnO_2 comes from an ESR investigation

published by Chang in 1980 [42]. The paper describes a reversible transformation of O_2^- into O^- witnessed at temperatures between 100 and 150 °C, shown in Figure 3. However, it was already pointed out that some of these assignments are inconsistent with both the theory and other ESR studies [16]; while a singlet was assigned to O^- in this study, theory shows that the signal should be a triplet [43], which is what was found for many other compounds, including closely related TiO_2 [44,45]. The analysis of ESR spectra is quite complicated, and there is no consensus on the assignment of some peaks; thus, there is no conclusive evidence of paramagnetic monoatomic oxygen species on SnO_2.

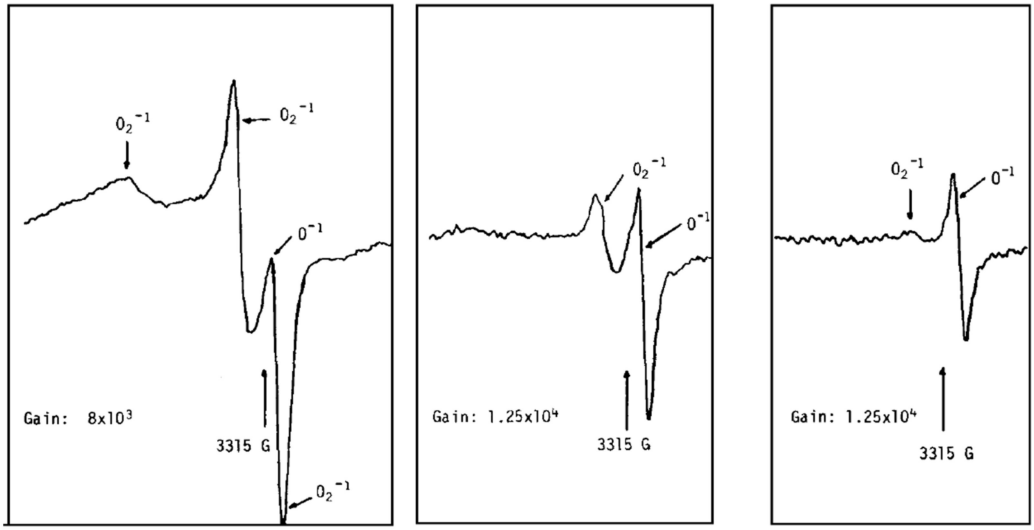

Figure 3. ESR spectra of SnO_2 in UHV. The sample was calcined in UHV at 550 °C for 4 h. (**a**) Sample at 20 °C. (**b**) The sample was warmed up to 100 °C. (**c**) The sample was warmed up to 150 °C. Reproduced with permission from Reference [42].

On the other hand, multiple ESR studies show triplet signals consistent with O_2^- adsorbates [46–49], which was confirmed by the appearance of the hyperfine structure in ^{17}O isotope exchange experiments [49]. This signal appears only on reduced surfaces, which have been heat-treated and cooled in UHV and exposed to O_2 below 150 °C, and its intensity is increased on Pt-doped surfaces [46]. These findings are in agreement with computational models of oxygen adsorption onto SnO_2, which only show adsorption on reduced surfaces [17,28,32]. However, ESR cannot provide evidence for the other computationally predicted species, the peroxide O_2^{2-}, which is not paramagnetic.

The existence of such low-temperature molecular adsorbates is also confirmed by TPD studies, which show that oxygen desorption from SnO_2 may be classified into three peaks, α, β and γ, as presented in Figure 4. The appearance of the α peak is correlated with low-temperature adsorption onto a surface preheated in vacuum at 700 and 550 °C (Figure 4a,b, respectively) for several hours and cooled down to below 150 °C before O_2 exposure. However, the peak does not appear if the sample was exposed to O_2 at temperatures above 300 °C; instead, two different desorption events occur, the β and γ peaks, which were assigned to O^- and lattice oxygen, respectively. However, the assignments are made based solely on the observed desorption temperatures. In one of the studies, the identity of the α and β adsorbates was investigated by ESR [50]; while α was confirmed to be O_2^-, no paramagnetic signal was detected for β. Therefore, the assignment of β as O^- is again doubtful, and other plausible explanations for the origin of β peak ought to be considered. It should also be pointed out that the onset and intensity of the β desorption peak depend not only on the pressure but also on the temperature at which oxygen dosing was performed [50–52]. Considering this and the fact that the peak coincides with the temperature range at which SnO_2 is known to reduce spontaneously [53], the β

peak could be explained by the desorption of O_{br} (surface reduction). Such assignment would also explain why the β peak does not appear after low-temperature dosing, where the chemisorbed oxygen species have insufficient energy to dissociate and heal the bridging vacancies. However, more data are necessary to make this determination conclusively.

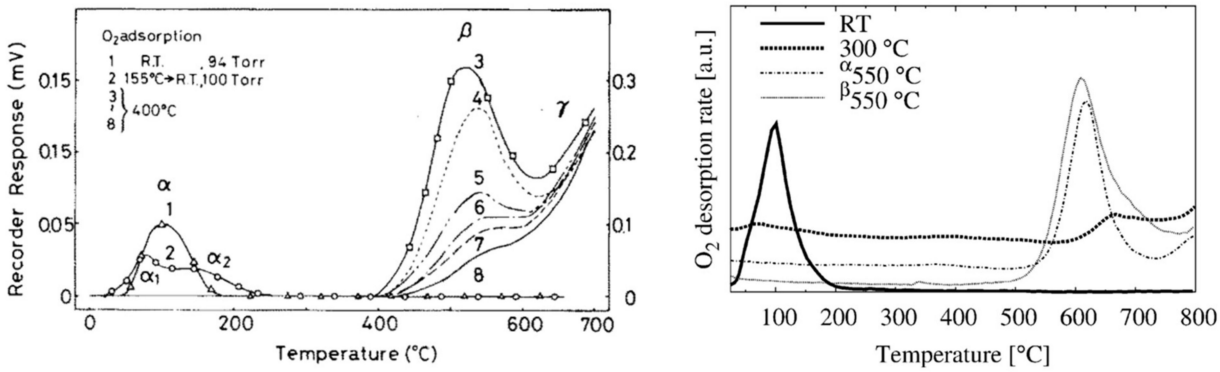

(**a**) (**b**)

Figure 4. TPD chromatograms of O_2 desorption from SnO_2. (**a**) Traces 1–2 correspond to the low-temperature adsorption following the evacuation at 700 °C. Traces 3–8 correspond to oxygen dosing at 400 °C and pressures of 99, 48, 16, 6, 3 and 2 Torr, respectively. Reproduced with permission from Reference [50]. (**b**) TPD of SnO_2 after exposure to O_2. Trace α denotes sample cooled in UHV, while β denotes cooling in O_2 background. Reproduced with permission from Reference [54].

The more recent evidence of adsorbed species comes from an operando DRIFTS study of O_2 and H_2 on a UHV treated sample, which is expected to have an appreciable initial density of vacancies. The spectra collected in several-minute intervals display emerging absorption bands attributable to superoxide and peroxide species [40]. The bands appear over the first few minutes and stabilise by about 15 min after gas introduction. If the atmosphere is then changed to H_2, the bands are removed rapidly over the first 5 min and disappear completely after just 10 min. Reintroduction of oxygen leads to the reappearance of the bands, showing the reversible formation of these adsorbates on reduced surfaces of SnO_2.

The development of near ambient pressure photoelectron analysers opened up the possibility of operando XPS analysis. Conveniently, the thermocouple lead of most NAP XPS systems can be used to measure the resistance of the sample in situ, therefore allowing analysis of a real, working sensor. The recent report of such an investigation does not show changes in the shape of O 1 s emission, which would have confirmed the presence of adsorbed species [19]. However, the spectra were collected at temperatures above 200 °C, so diatomic adsorbates (α peak in TPD) were unlikely to persist at the surface. On the other hand, a rigid shift in the binding energy (BE) scale was observed for all core levels, suggesting a change in the Fermi level of the sample, which is evidence of band bending. The peaks shift to lower BE in the O_2 atmosphere relative to UHV, which the authors interpret as evidence of upward band bending caused by chemisorbed oxygen. However, another possible interpretation of the observed Fermi level change stems from a different choice of reference. The formation of vacancies in SnO_2 introduces shallow electron donors, which may become thermally ionised and cause downward band bending. This would manifest itself as a shift of peaks to higher BE in photoelectron spectroscopy, which was observed in both UPS and XPS on reduced and oxidised SnO_2 samples [53]. These authors conclude that the flat band condition corresponds to a perfect, stoichiometric surface on which no adsorbates can exist, and the bands bend downward from that, moving peaks in both UPS and XPS spectra to higher binding energies.

4. Interactions with Reducing Gases

4.1. Ionosorption Based Models—Reactions with Preadsorbed Oxygen

Since the foundations of oxygen ionosorption were established, the detection of reducing gases was understood in terms of the reaction with surface oxygen ions and the release of electrons trapped at the surface into the conduction band. The papers on the detection of common reducing gases, such as CO, H_2 or VOC, describe the surface reactions in a manner presented in Table 1.

Table 1. Reactions of common reducing gases with ionosorbed oxygen.

Reaction	References
$CO + O^- \rightarrow CO_2 + e^-$	[8,55,56]
$H_2 + O^- \rightarrow H_2O + e^-$	[50,57–60]
$VOC + nO^- \rightarrow xCO_2 + yH_2O + ne^-$	[4,61,62]

Similar to the core theory behind them, these mechanisms do not refer to the adsorption configurations of the species involved. As discussed earlier, computational studies suggest that O^- cannot be implicitly assumed to exist, and empirical studies systematically fail to show O^- on SnO_2, suggesting that these reactions may be an oversimplification that defines a particular stoichiometry for the surface processes rather than defining the involvement of specific adsorbed species.

In the previous chapter, the adsorption configuration of an oxygen molecule onto a V_{br} was discussed. Computational studies show that various combustible gases, such as CO and NO, can adsorb on top of an O_2 molecule and subsequently react with it [17,28,30,32]. On both the (110) and (101) surfaces, one half of the dioxygen heals a V_{br}, and the other reacts with the combustible molecule, as shown in Figures 5 and 6.

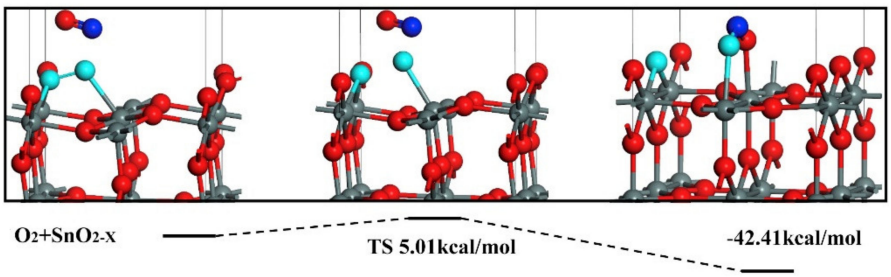

Figure 5. Coadsorption of NO and O_2 onto a reduced (110) surface of SnO_2. Reproduced with permission from Reference [30].

By the example of CO, the overall process occurring at a vacancy can therefore be described as:

$$V_O^{\cdots} O_2^- + CO \rightarrow O_O + CO_2 + e^-$$

Similar to the O^- based detection in Table 1, this process involves releasing one electron per molecule detected; however, it is described by a species known to exist on SnO_2, and the calculated transition state energies are reasonably low (0.80 eV on the (110) surface and 0.43 eV on the (101) surface) [17,32]. The products of the reactions are initially adsorbed but may either desorb or further react with the surface. The latter possibility is explored below.

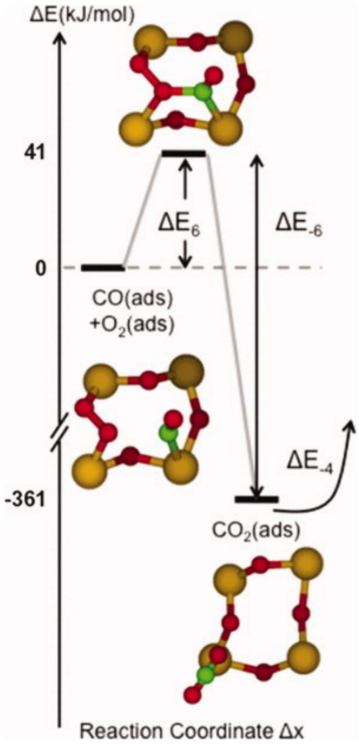

Figure 6. Coadsorption of CO and O_2 onto a reduced (101) surface of SnO_2. CO reacts with O_2 preadsorbed onto a V_O. Reproduced with permission from reference [32].

While the reaction of CO and NO with preadsorbed oxygen species leads to the healing of a surface oxygen vacancy, the coadsorption of O_2 and H_2 is predicted to look quite different. In this case, one hydrogen atom binds to each of the adsorbed dioxygen atoms to form two distinct hydroxyl groups [63]. Hydrogenation of the oxygen atom bound to the V_O results in a rooted hydroxyl ($(OH)_O$), which occupies the bridging lattice site, while the other oxygen atom becomes a terminal hydroxyl bound to a neighbouring Sn_{5c} site ($Sn_{5c} \cdots OH$). The two hydroxyl groups have dissimilar properties and hence affect the electronic structure of SnO_2 differently [59]. The $Sn_{5c} \cdots OH$ hydroxyl forms a dipole, and it does not contribute to the sensor's resistance other than by removing the oxygen adsorbate during hydroxyl formation. On the other hand, the $(OH)_O$ is an electron donor (relative to the equivalent O_{br} it replaces), which can donate charge carriers to the conduction band and become positively charged; the formation of such hydroxyl surface donors is expected to have a noticeable effect on the sensor's resistance [58,59,64].

Although these mechanisms show how reducing gases may be detected on the surfaces of SnO_2, they do not provide the complete picture. If a sensor's resistance were regulated solely by the formation and consumption of oxygen adsorbates, then the lowest attainable resistance would be in the absence of oxygen. However, it was shown experimentally that the resistance of a sensor might fall below the no-oxygen baseline during CO detection in humid synthetic air [64]. Therefore, mechanisms extending beyond the interaction with preadsorbed oxygen need to be considered.

4.2. Direct Adsorption of Reducing Gases

Humidity is virtually always present in the atmosphere in varying amounts, which is a potential problem for the reliability of gas sensors, as the adsorption of water could cause the resistance of a sensor to change. Computational studies show that the interaction between the surface and H_2O is complex; many adsorption configurations are possible, including both molecular and dissociative modes, as shown in Figure 7.

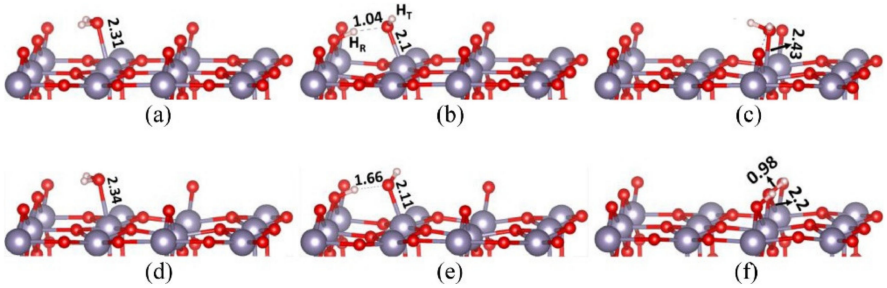

Figure 7. Adsorption of H_2O onto (**a**,**b**) stoichiometric and (**c**–**f**) reduced (110) surfaces of SnO_2. Adsorption energies are given for each configuration. (**a**) Molecular adsorption onto Sn_{5c}, −1.29 eV. (**b**) Dissociative adsorption on Sn_{5c}, −1.85 eV. (**c**) Molecular adsorption onto Vbr, −0.81 eV. (**d**) Molecular adsorption onto Sn_{5c} with a neighbouring V_{br}, −1.32 eV. (**e**) Disscheme 5. $_c$ with a neighbouring V_{br}, −1.92 eV. (**f**) Dissociative adsorption on V_{br}, −2.48 eV. Reproduced with permission from Reference [29].

On a stoichiometric surface, H_2O can adsorb onto an Sn_{5c} site [29]. The adsorption energy is relatively small compared to other possible configurations but can be further lowered by the dissociation of the H_2O molecule, where one of the H atoms coordinates to a neighbouring O_{br}. The remaining OH coordinated to the Sn_{5c} becomes a terminal hydroxyl ($Sn_{5c}\cdots OH$), and the reaction of O_{br} with H atom transforms it into a rooted hydroxyl ($(OH)_O$); an example of such an interaction is shown in Figure 7b. In fact, the result of dissociative adsorption of H_2O on a stoichiometric surface is quite similar to the reaction of H_2 with preadsorbed O_2, as discussed above.

The formation of an oxygen vacancy on the surface strongly influences the adsorption of H_2O; the adsorption energy of H_2O onto an Sn_{5c} is more negative on a surface with a V_{br} in the vicinity, both in the molecular and dissociative configurations [29]. However, the vacancy is also a new adsorption site for H_2O, leading to more stable species. Although molecular adsorption onto V_{br} is the least stable of all configurations, the dissociative mode on V_{br}, as shown in Figure 7f, is the opposite, being the most favourable adsorption configuration of all. This configuration is also unique in that it produces two $(OH)_O$ instead of one of each type of hydroxyl. Therefore, it should affect the resistance more strongly as two electron donors are formed per molecule detected instead of one [29,65].

Although dissociative adsorption is more stable than its molecular counterpart on both adsorption sites, H_2O cannot always spontaneously dissociate upon adsorption. The process was shown to be thermally activated in an operando DRIFTS study, where the appearance of bands corresponding to OH was observed only after dosing H_2O at temperatures above 200 °C [66].

The preferred adsorption mode of H_2O, therefore, depends strongly on the surface of SnO_2, which determines the range of possible configurations based on the availability of adsorption sites, for example neighbouring V_{br} and O_{br}, to allow dissociative adsorption. This may not necessarily be a common occurrence, as the bridging vacancies tend to group together, for example, in the proposed structure of the 2 × 1 reconstruction of the (110) surface, where every other row of bridging oxygen atoms is removed. This suggests that depending on the preparation, the surfaces should behave differently in the presence of humidity, which was shown experimentally in an H_2O/D_2O exchange study using DRIFTS [67]. The study also confirms that SnO_2 surface hydroxylation is a reversible process in a dynamic equilibrium with the gas phase. Additional TPD data show that H_2O desorbs from the surface over a wide range of temperatures, suggesting multiple adsorption configurations with different adsorption energies [51,52]. The TPD chromatograms (Figure 8) show two broad peaks, one around 100 °C, which corresponds to molecularly adsorbed water, and another above 400 °C, which results from various dissociatively adsorbed species. Since the adsorption energy decreases with increasing

OH coverage, it takes progressively more energy to desorb H_2O from SnO_2, which is why temperatures of at least 600 °C are required for complete dehydroxylation [66].

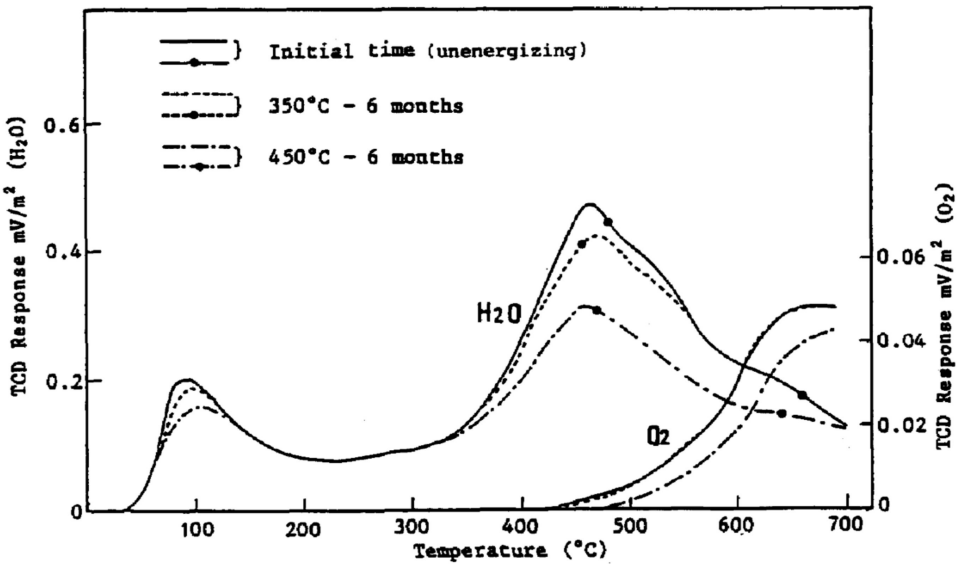

Figure 8. TPD chromatograms of H2O and O2 desorption from SnO2. Reproduced with permission from Reference [51].

An operando DRIFTS study with simultaneous resistance measurements reveals that H_2O does not always induce a reducing response. [67]. Two differently prepared samples of SnO_2 were exposed to increasingly humid synthetic air. While one of the samples shows a strong response, the effect of humidity on the other sample is negligible. However, spectra reveal that the former is accompanied by relatively small changes in the OH bands, while intense OH formation is observed for the latter. Therefore, experimental data suggest that there must be two adsorption mechanisms, one which causes a reducing type response, likely linked to the formation of $(OH)_O$ electron donors, and one which is relatively electroneutral, which could be dominated by the formation of $Sn_{5c} \cdots OH$ [59].

Although ionosorption is the prevalent sensor operation mechanism discussed in the literature, it has been known for a long time that CO elicits a response on SnO_2-based sensors in the absence of oxygen [56]. Since no CO_2 was observed during CO adsorption in the absence of O_2, the change in resistance was attributed to the direct adsorption of CO onto SnO_2, which produces a surface donor state that can become ionised by donating an electron into the conduction band, increasing the sensor's resistance. The authors support their argument with the study of Heiland et al., who studied the interactions of SnO_2 with acetic acid by TPD [68]. According to the TPD results, the reaction products desorb from the surface primarily as CO instead of CO_2, which Hahn interprets as a lack of reaction between CO and the surface. However, these results are at odds with the findings of Yamazoe et al., who recorded TPD chromatograms after dosing CO, rather than acetone, onto SnO_2 powder. They found only CO_2 desorbing from the surface and concluded that CO irreversibly adsorbs onto SnO_2 and desorbs as CO_2 upon heating, suggesting the reaction follows a Mars-van Krevelen mechanism [69]. Therefore, it is likely that multiple adsorption pathways for CO are possible.

It is well known that humidity has a substantial impact on the detection of CO in SnO_2-based gas sensors. One of the possible contributory processes is the transformation of O_{br} into $(OH)_O$ when a CO molecule reacts with a terminal OH, which was found on a (101) surface [32]. The initial and final adsorbate configurations and the transition state are shown in Figure 9. Although the process forms a donor state, which will influence the sensor's resistance, it permanently removes important adsorption sites for CO, as explained in the next section.

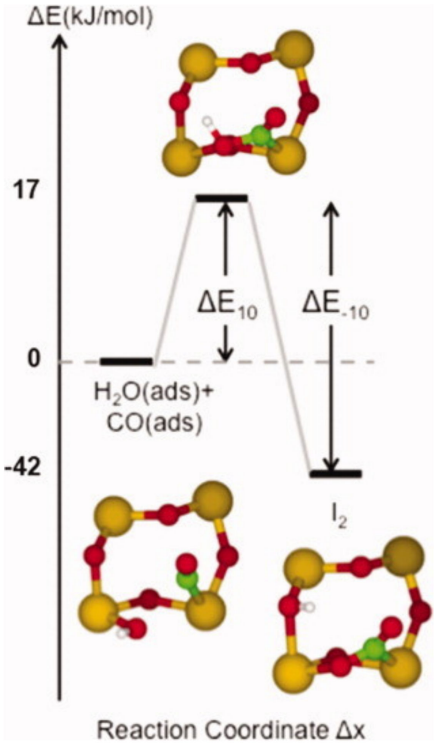

Figure 9. Adsorption of CO onto a (101) surface of SnO_2 with a terminal hydroxyl on an adjacent Sn_{5c} site. Reproduced with permission from Reference [32].

Computational investigation of NO adsorption onto SnO_2 reveals that various geometries are possible, but the most stable ones are linked to nitrogen (N^-)down configurations [30]. Contrary to H_2O adsorption, the bonding interaction between NO and Sn_{5c} is more favourable on a stoichiometric surface than on a reduced one. However, when present at the surface, the V_{br} is again the preferred adsorption site. Although a different study reports no O-down geometries [18], both studies agree that the most stable adsorption configuration is N-down onto a V_{br} with an adsorption energy of about 1.2 eV. Analysis of the charge density transfer reveals that, in terms of the influence on the electronic structure, NO can act not only like a reducing gas but also like an oxidising one [18]. While adsorption onto O_{br} results in a donor-like NO^+ state, the same molecule adsorbing onto a V_{br} results in electron density being withdrawn from the surface and the formation of an NO^-. Effectively, NO adsorption will produce a reducing gas response on a stoichiometric surface but an oxidising gas response on a fully reduced surface. For intermediate surfaces, a mixture of the adsorbates is expected at the surface; such behaviour complicates NO detection.

The detection mechanisms of many gases involve their transformation into reaction products such as H_2O (from H_2), NO_2 (from NO) and CO_2 (from CO). Of these, the formation of H_2O is usually lost in the background humidity, but the ambient concentrations of CO_2 and NO_2 are respectively small and negligible, which means that their interference should be taken into consideration. NO_2 is considered an oxidising gas, which strongly increases the resistance of the sensor. Its adsorption is discussed in the next section.

On the other hand, CO_2 seems to have little effect on the sensor's resistance compared to other gases; considerable concentration changes produce a relatively small response. A computational study found that CO_2 does not adsorb onto a stoichiometric (110) surface of SnO_2, as only very weak interactions were found [70]. Moreover, on a reduced (110) surface with preadsorbed $V_O \cdots O_2$, the CO_2 does not interact with O_2, as the two molecules are localised far apart from each other in their equilibrium position. These two conclusions imply that CO_2 should not substantially affect the sensor's resistance, as they eliminate two

main detection mechanisms. However, a different study suggests the possibility of CO_2 adsorption on a stoichiometric (101) SnO_2 surface, with the molecule coordinating to an O_{br} and two Sn_{5c} sites in a tridentate carbonate form, as shown in Figure 10 [32]. A charge transfer occurs from the surface, with each forming carbonate gaining 0.120 e^-, determined from population analysis. Moreover, it was shown that the (110) surface could also be activated towards CO_2 detection; an investigation of CO_2 adsorption onto a hydroxylated surface shows a possible reaction leading to the formation of a bidentate carbonate ion adsorbed onto two Sn_{5c}, with the remaining H atom coordinating to a neighbouring O_{br} to form an $(OH)_O$. It appears that the presence of $Sn_{5c} \cdots OH$ also activates neighbouring O_{br} to react with CO_2 forming a bidentate CO_3^{2-} between an Sn_{5c} and V_{br}. These findings show how humidity should enhance the sensing properties of SnO_2 towards CO_2, which has been demonstrated experimentally [70]. However, because of the poor performance of pure SnO_2 in CO_2 detection, most studies involve modification of the surface, for example, by lanthanum doping [71,72], and relatively few studies investigate the interaction of CO_2 with undoped SnO_2.

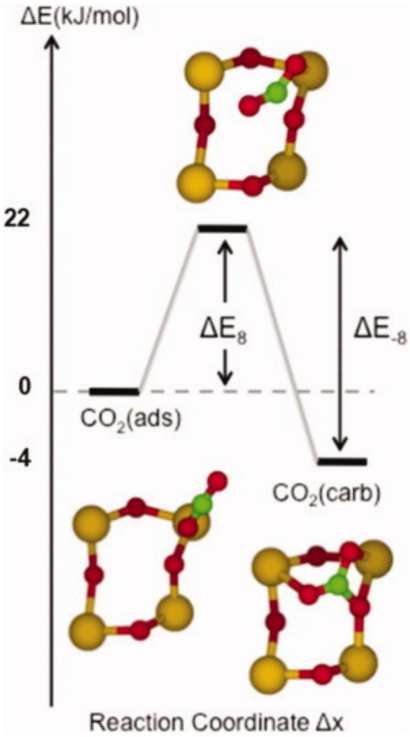

Figure 10. Adsorption of CO_2 onto a stoichiometric (101) surface of SnO_2. The formed adsorbate is a tridentate carbonate-like species. Reproduced with permission from Reference [32].

4.3. Reduction of the Surface

There is another reaction pathway for detecting CO, which recently has gained more recognition within the gas sensing community. As mentioned before, the direct reduction of the SnO_2 surface by CO was initially discounted as no CO_2 was detected in the outflowing gas [56]. However, such behaviour would vary significantly from many other oxides, on which CO oxidation proceeds via a Mars-van Krevelen (MvK) mechanism, which features a cyclic reduction/oxidation of the adsorption sites [73,74]. Indeed, DFT studies on various SnO_2 surfaces have shown repeatedly that the direct reduction of the surface by CO should also be possible [17,28,32,75]. Several mechanisms were proposed, through which the CO molecule may react with O_{br}, for example, through a carbonate intermediary, as shown in Figure 11.

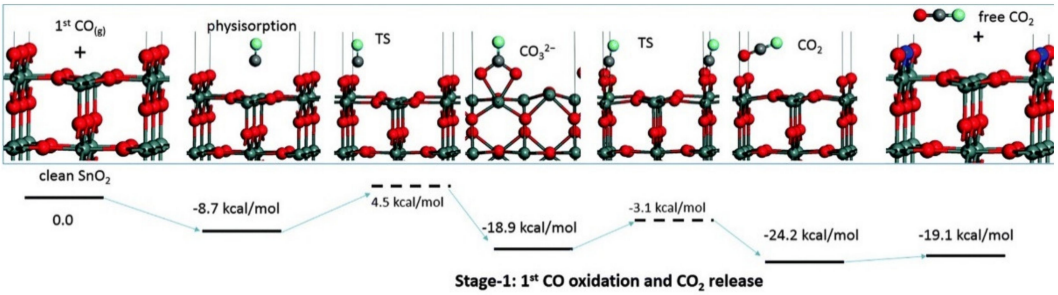

Figure 11. Direct reduction of the (110) surface of SnO_2 during CO adsorption. Reproduced with permission from Reference [17].

Although the formation of a carbonate species on the surface is often associated with CO detection, it is likely a secondary process resulting from the adsorption of the produced CO_2. Experimentally, it was found that carbonates do not always appear during CO dosing on SnO_2 and that identical features in the DRIFTS spectra may be produced by dosing CO_2 instead of CO [76]. Indeed, the formation of surface carbonates seems to be related to the immediate sample pre-treatment, with the species appearing after preparation at 450 °C but not after 1000 °C [67,76].

Whether the carbonates are formed during or after the interaction of SnO_2 with CO, the predicted reduction of the surface by CO was confirmed experimentally in operando UV-Vis diffuse reflectance spectroscopy [77]. The analysis revealed strong absorption in the visible region upon dosing with CO, consistent with the formation of in-gap electronic states of oxygen vacancies, making the typically transparent semiconductor opaque. Additional evidence comes from a TPD study, which shows that CO desorbs from the SnO_2 surface almost exclusively as CO_2, which indicates that CO reacts with the surface upon adsorption [69]. Moreover, the amount of CO_2 desorbed after CO dosing depends strongly on the degree of surface reduction, and therefore the density of O_{br} (versus V_{br}) on the surface. This indicates that surface oxygen atoms are important adsorption sites and that non-reductive adsorption of CO onto SnO_2 is limited. Therefore, there is strong experimental evidence supporting this mechanism of gas–surface interactions.

It seems fortuitous that CO can reduce the surface of SnO_2 directly by reacting with O_{br}; the V_{br} are essential adsorption sites for oxygen that enable the secondary reaction of CO with the preadsorbed oxygen, reforming the O_{br} lost in the reduction. This cyclic process results in a dynamically changing density of O_{br} on the surface. The steady-state coverage, which eventually determines the electronic properties of the surface, will depend on the rates of reduction and oxidation, and therefore the concentration of CO, assuming the ambient oxygen concentration is constant. Because of the strong evidence supporting the reaction, it is more reasonable to perceive the detection mechanism of CO in terms of plausible reactions of well-established species rather than an elusive monoatomic adsorbate; such descriptions of CO detection have been proposed recently [76], which foreshadows a new era in gas-sensor modelling.

Although the reactant geometry of the reduction of SnO_2 by NO is similar to CO, the reaction is less likely in the case of NO. DFT calculation determined that this process is endothermic, making it less likely to occur at noticeable rates [30]. Nevertheless, there is a possibility of a direct surface reduction by NO, which results in the formation of NO_2 adsorbed onto a bridging vacancy. The production of this interfering gas is somewhat problematic, as it is an oxidising gas that causes a significant increase in the sensor's resistance. The adsorption mechanisms of NO_2 are the subject of the following section.

5. Interactions with Oxidising Gases—NO_2

5.1. Adsorption onto Stoichiometric Surfaces

Even though oxygen lends its name to this category of target gases, it rarely is considered one, as it defines the baseline resistance of sensors. Therefore, oxidising gases are

those that increase the sensor's resistance relative to an ambient oxygen background, for example, NO_2 or SO_2. The current research focuses on the former, and there is very little research on other oxidising gases, with SO_2 sometimes included as a frequent interfering gas to NO_2.

Conventionally, NO_2 detection is considered in terms similar to oxygen ionosorption; the adsorbates withdraw electrons from the conduction band of SnO_2. However, the formed states are deeper than those of oxygen, causing stronger band bending and a more significant resistance increase [78]. Even though this description is fairly straightforward, the reactions of NO_2 on the surface of SnO_2 seem to be quite complex. In contrast to carbon, which only forms two oxides, nitrogen can form a variety of oxides, such as N_2O, NO, NO_2, N_2O_4 and the NO_3^- ion, many of which are formed during parasitic reactions on the surface of the sensor [78] as evidenced by IR and Raman spectroscopic analyses [66,79]. Long sensor recovery time, during which conductivity of the sensing layer returns to its baseline value after removal of the target gas, has been linked to the formation of the NO_3^- ion, which has significantly larger adsorption energy than NO_2, and therefore desorbs at a slower rate [80]. In order to improve the performance of sensors, it is crucial to understand the formation mechanisms of various nitrogen oxides on the surfaces of SnO_2 and to design sensitive layers that could hinder parasitic reactions.

On stoichiometric SnO_2 (101) surfaces, NO_2 can adsorb in a monodentate or bidentate bridging geometry with one or two neighbouring Sn_{5c} sites [81]. The adsorption energy between the two configurations differs by only about 0.13 eV. It means that even at room temperature, the molecule should convert easily between the two states, which would result in a "random walk" along the Sn_{5c} rows. This could eventually lead to two NO_2 molecules happening upon one another at the surface, resulting in them reacting; one of the molecules abstracts an oxygen atom from the other to become an NO_3^- ion, while the other is reduced to NO, which may adsorb onto a neighbouring site or desorb from the surface. The occurrence of this reaction is supported by the observation of an intermediate NO_2 dimer, denoted as $ONONO_2$, using in-situ Raman spectroscopy [79].

Whereas the interaction of SnO_2 with the produced NO is relatively weak, the NO_3^- adsorbs much more strongly than NO_2. Contrary to NO_2, the energy difference between the monodentate and bridging geometries of NO_3^- is considerable [81]; therefore, a random walk along the Sn paths is unlikely. Moreover, because of the stronger adsorption of NO_3^-, temperatures of up to 700 °C are necessary to remove the adsorbates altogether. In terms of their electronic effects, the Bader charge trapped by the NO_3^- is over twice as large as that trapped by an adsorbed NO_2 molecule, which suggests it should affect the sensor's resistance much more strongly [80]. As a result, the formation of NO_3^- may lead to sensor poisoning and long recovery times.

5.2. Adsorption onto Reduced Surfaces

Although a "walking" NO_2 molecule is interesting to picture, the preferable adsorption site for this gas is a surface oxygen vacancy, as shown in independent computational studies [18,31]. The molecule interacts with a vacancy via the oxygen atoms. Both studies determined that NO_2 adsorption onto a bridging vacancy is stronger than at an in-plane vacancy. NO_2 adsorbed onto V_{br} is most stable in a monodentate configuration, though bidentate geometries coordinated to a nearby Sn_{5c} or another V_{br} are also possible. In all such geometries, the molecule is immobile, which lowers its chance of reacting with another NO_2 to form nitrates. Many studies highlight the importance of oxygen vacancies in the low-temperature detection of NO_2 on SnO_2-based gas sensors, although they sparsely comment on the atomistic origin of the superior sensitivity [82–84].

Adsorption onto an oxygen-deficient surface offers a reaction pathway that is unavailable on a stoichiometric one, which is the dissociation of NO_2, as shown in Figure 12. We have already considered the mechanism by which reducing gases affect the sensor's resistance; the current process can be thought of as the direct opposite. Similar to oxygen, the adsorption of NO_2 at a surface vacancy can lead to the oxidation of the surface, as

shown in a computational study of the (110) surface [18]. The adsorption of NO_2 onto V_{br} leads to the dissociation of the molecule and healing the vacancy; the authors comment on the likeness between the final structure achieved here and during the adsorption of NO onto a stoichiometric surface. Therefore, apart from the electron-withdrawing properties of NO_2 adsorption, the removal of V_O self-doping in SnO_2 must be considered. Moreover, the molecule preferentially heals the bridging oxygen site on a surface where in-plane vacancies are also available, in agreement with the preferable adsorption onto O_{br}. This selectivity is inverted in the case of SO_2, which preferentially adsorbs onto V_{pl} [31]. Therefore, in theory, one can regulate the selectivity of a sensor by selectively creating bridging vacancies.

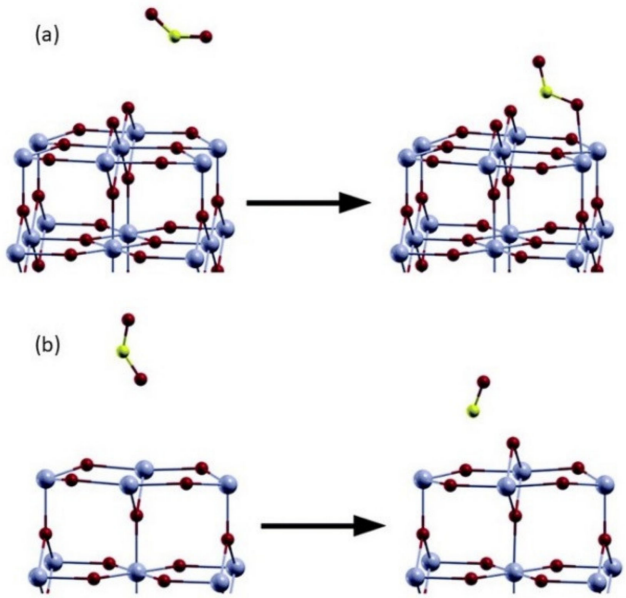

Figure 12. Adsorption of NO_2 onto (110) surface of SnO_2. (**a**) Stoichiometric surface, monodentate adsorption onto Sn_{5c}. (**b**) Reduced surface, dissociative adsorption onto a V_{br}, leading to the healing of the vacancy and an adsorbed NO molecule. Reproduced with permission from Reference [18].

Adsorption of NO_2 onto SnO_2 with various distributions of both bridging and in-plane vacancies was studied via first-principles thermodynamics, and the results show clearly that bridging vacancies are the more favourable of the two [85]. Based on these results and the Redhead equation, a simulated TPD chromatogram was computed and compared to experimental data, as shown in Figure 13. The match is reasonable, although experimental data show some high-temperature desorption of NO, which was not predicted by DFT. Moreover, the empirical TPD study that benchmarks simulated desorption shows NO desorption only at temperatures above 200 °C on a differently prepared surface [66]. This could be explained by a temperature-activated dissociation of NO_2 at a surface vacancy, resulting in NO desorbing at temperatures above typical, which the DFT study did not consider. However, it should be mentioned that while the desorption is dominated by NO_2 in this study, an earlier TPD study found only NO and some N_2O desorbing from SnO_2 powder after adsorption at room temperature [69]. This interesting difference, if confirmed, could indicate the importance of the atomistic state of the surface in determining its interactions with gas adsorbates.

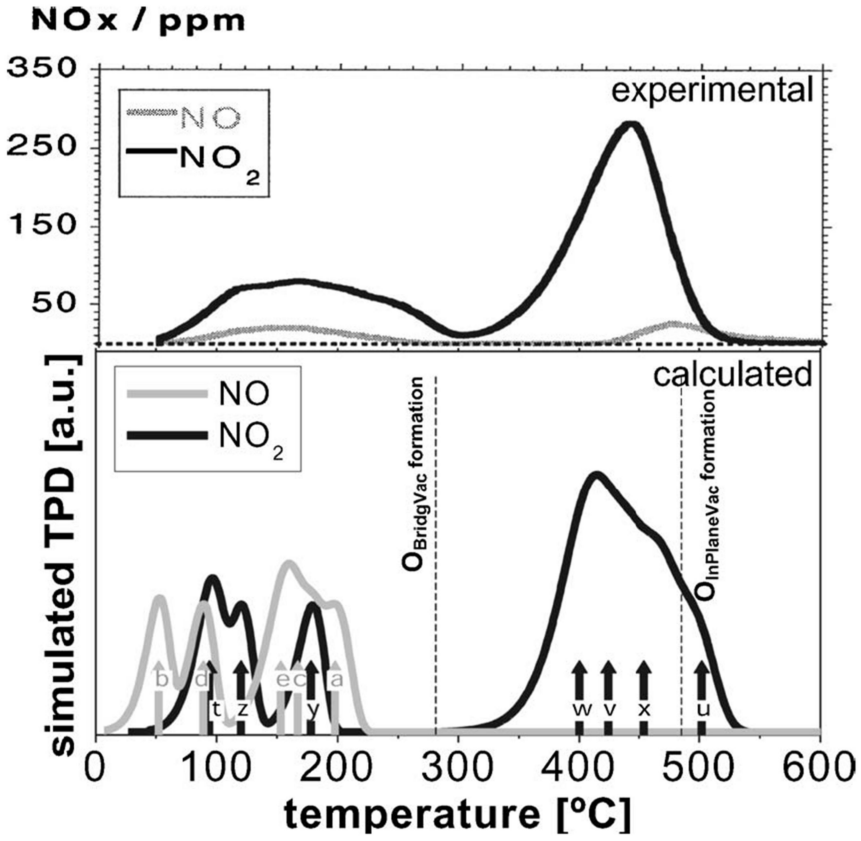

Figure 13. Comparison of empirical and simulated NOx desorption in TPD of SnO_2 after exposure to NO_2. Reproduced with permission from Reference [85].

6. Oxygen Vacancies versus Gas Sensing Mechanism

The previous chapters discussed the importance of oxygen vacancies as adsorption sites, their formation during the interaction with reducing gases, and their healing via the complex interactions with oxygen or oxidising gases. However, as mentioned before, oxygen vacancies are also a crucial self-doping mechanism of SnO_2 and largely determine its intrinsic conductivity [24]. Although a detailed description of the involvement of V_O in the transducer function of gas sensors is beyond the scope of this review, there are several points worth considering.

Even though oxygen vacancies have long been recognised as the source of conductivity in bulk SnO_2, recent computational studies show these electronic states to be deep in the bandgap, thus unlikely to contribute to conductivity [23]. Moreover, the defects are now considered negative-U type, where the attractive interaction between two electrons bound at a vacancy means that the system's energy with a singly occupied vacancy can be lowered by capturing a conduction electron at the defect [23]. By implication, singly ionised vacancies are not thermodynamically stable for any Fermi level position [86]. This computational finding contradicts the well-established evidence of paramagnetic (singly occupied) oxygen vacancies observed in ESR studies [22,46], which could hint at a difference between the nature of bulk and near-surface vacancies. The effect of vacancies on the electronic properties of SnO_2 could depend on their depth below the surface, with bulk vacancies being energetically deep, negative-U and likely neutral, and surface vacancies singly or doubly ionised depending on the temperature. The singly charged vacancies, which could emerge in the substoichiometric coordination of a reduced surface, should then lead to the formation of a surface conductivity layer, while the bulk of the material remains an insulator (relative to the surface). Indeed, such surface conductivity layer models have been proposed recently for In_2O_3, a gas-sensitive material analogous to SnO_2,

whose conductivity as a thick particulate film is several times larger than bulk conductivity models can account for [87].

The existence of singly ionised vacancies is important to acknowledge, as it reveals certain parallelism between ionosorption and surface reduction. If the formed oxygen vacancy is a singly ionised donor, the conduction band has gained one electron per lattice oxygen atom lost, similar to the formation of O^-. Moreover, such interpretation of the meaning of phenomenological "ionosorbed oxygen" could explain why some studies observe macroscopic changes consistent with the appearance of ionosorbed O^{2-} at elevated temperatures, even though such species are known to be unstable outside of the stabilising influence of the Madelung potential on oxygen lattice sites.

7. Conclusions

The insight provided by recent molecular modelling studies, backed by emerging operando spectroscopy, offers a new perspective on the gas-sensitive phenomena of SnO_2-based gas sensors, and therefore our understanding of the sensing mechanisms needs to be re-evaluated. Although the prevalent model of oxygen ionosorption can explain some of the observed macroscopic behaviour of the sensors, it is based on species thus far unconfirmed. The systematic lack of evidence after so many years of research indicates that new mechanisms need to be considered.

The only convincing evidence of oxygen adsorbates on the SnO_2 surface is linked to diatomic species, whose effect on the sensor's resistance is limited according to ionosorption theory, which requires O^- to work. Although O^- may exist under special circumstances, most interactions between the surface, O_2 and target gases are mediated by the diatomic oxygen adsorbates. It is important to mention that both the dissociation of O_2 and the reaction of a target gas with preadsorbed oxygen results in the healing of a surface vacancy, which should affect the equilibrium density of vacancies, providing a mechanism for resistance change.

Furthermore, direct evidence of the reduction of the SnO_2 surface was finally obtained, which settles the debate of whether CO can react with the O_{br}, as predicted for some years based on DFT calculations. The lack of CO_2 observed during the dosing of CO on SnO_2 in the absence of oxygen is then somewhat puzzling but could be explained by a slow rate of reaction and the depletion of O_{br}, which cannot be replenished by ambient oxygen. This is supported by the strong dependence on the amount of desorbed species after CO dosing based on the degree of surface reduction.

The importance of bridging sites is further highlighted in the adsorption mechanisms of H_2O. O_{br} is a reaction partner for the dissociation of H_2O on both reduced and stoichiometric surfaces, and the dissociation on a V_{br} leads to the formation of an additional electron donor, thus causing a larger resistance change. Moreover, the transformation of O_{br} into $(OH)_O$ is the most likely candidate for the interference in CO detection, as the essential adsorption site is removed.

Finally, the bridging sites are heavily involved in the detection of both NO and NO_2, which transform into one another in a network of complex interactions with the surface. In the process, they either form or heal bridging vacancies, which should strongly affect the baseline conductivity of SnO_2. However, these two gases also adsorb readily onto various other sites, which should also have a noticeable effect on the sensor's resistance. The mutual coexistence of the absorbed species in these processes is evidenced by the results of the adsorption of one or the other, which leads to a similar final state, as noticed independently by both computational and empirical scientists.

In conclusion, the majority of evidence points to the mechanisms centred around oxygen vacancies. The surface of SnO_2 is a dynamic assembly, which can support a large density of vacancies both at the surface (bridging and in-plane) and in several atomic layers below the surface. As evidenced by experimental studies, the in-plane oxygen vacancies play an important role in determining its conductivity and reactivity. Therefore, the surface of SnO_2 is an exchange zone between bulk and gas-phase oxygen, and the sensors response

can be seen as resulting from the change in the position of the exchange equilibrium, on top of which the effects of direct adsorption may manifest as additional resistance change.

Funding: This work was supported by the Engineering and Physical Sciences Research Council (EP/R512400/1).

Conflicts of Interest: The authors declare no conflict of interest.

References

1. Rieu, M.; Camara, M.; Tournier, G.; Viricelle, J.P.; Pijolat, C.; de Rooij, N.F.; Briand, D. Fully Inkjet Printed SnO_2 Gas Sensor on Plastic Substrate. *Sens. Actuators B Chem.* **2016**, *236*, 1091–1097. [CrossRef]
2. Devabharathi, N.; Umarji, A.M.; Dasgupta, S. Fully Inkjet-Printed Mesoporous SnO_2-Based Ultrasensitive Gas Sensors for Trace Amount NO_2 Detection. *ACS Appl. Mater. Interfaces* **2020**, *12*, 57207–57217. [CrossRef]
3. Zhang, Q.; Zhou, Q.; Lu, Z.; Wei, Z.; Xu, L.; Gui, Y. Recent Advances of SnO_2-Based Sensors for Detecting Fault Characteristic Gases Extracted from Power Transformer Oil. *Front. Chem.* **2018**, *6*, 1–7. [CrossRef]
4. Zhang, Z.; Huang, K.; Yuan, F.; Xie, C. Gas Sensing Properties and in Situ Diffuse Reflectance Infrared Fourier Transform Spectroscopy Study of Acetone Adsorption and Reactions on SnO_2 Films. *Sens. Mater.* **2014**, *26*, 649–663. [CrossRef]
5. Meng, X.; Zhang, Q.; Zhang, S.; He, Z. The Enhanced H_2 Selectivity of SnO_2 Gas Sensors with the Deposited SiO_2 Filters on Surface of the Sensors. *Sensors* **2019**, *19*, 2478. [CrossRef] [PubMed]
6. Wang, W.; Zhang, Q.; Lv, R.; Wu, D.; Zhang, S. Enhancing Formaldehyde Selectivity of SnO_2 Gas Sensors with the ZSM-5 Modified Layers. *Sensors* **2021**, *21*, 3947. [CrossRef]
7. Ding, J.; McAvoy, T.J.; Cavicchi, R.E.; Semancik, S. Surface State Trapping Models for SnO_2-Based Microhotplate Sensors. *Sens. Actuators B Chem.* **2001**, *77*, 597–613. [CrossRef]
8. Bârsan, N.; Hübner, M.; Weimar, U. Conduction Mechanisms in SnO_2 Based Polycrystalline Thick Film Gas Sensors Exposed to CO and H2 in Different Oxygen Backgrounds. *Sens. Actuators B Chem.* **2011**, *157*, 510–517. [CrossRef]
9. Barsan, N.; Weimar, U. Conduction Model of Metal Oxide Gas Sensors. *J. Electroceramics* **2001**, *7*, 143–167. [CrossRef]
10. Morrison, S.R. Mechanism of Semiconductor Gas Sensor Operation. *Sens. Actuators* **1987**, *11*, 283–287. [CrossRef]
11. Heiland, G. Homogeneous Semiconducting Gas Sensors. *Sens. Actuators* **1981**, *2*, 343–361. [CrossRef]
12. Geistlinger, H. Electron Theory of Thin-Film Gas Sensors. *Sens. Actuators B Chem.* **1993**, *17*, 47–60. [CrossRef]
13. Göpel, W.; Schierbaum, K.D. SnO_2 Sensors: Current Status and Future Prospects. *Sens. Actuators B Chem.* **1995**, *26*, 1–12. [CrossRef]
14. Hauffe, K. The Application of the Theory of Semiconductors to Problems of Heterogeneous Catalysis. *Adv. Catal.* **1955**, *7*, 213–257. [CrossRef]
15. Pulkkinen, U.; Rantala, T.T.; Rantala, T.S.; Lantto, V. Kinetic Monte Carlo Simulation of Oxygen Exchange of SnO_2 Surface. *J. Mol. Catal. A Chem.* **2001**, *166*, 15–21. [CrossRef]
16. Gurlo, A. Interplay between O_2 and SnO_2: Oxygen Ionosorption and Spectroscopic Evidence for Adsorbed Oxygen. *Chem. Phys. Chem.* **2006**, *7*, 2041–2052. [CrossRef]
17. Lu, Z.; Ma, D.; Yang, L.; Wang, X.; Xu, G.; Yang, Z. Direct CO Oxidation by Lattice Oxygen on the SnO_2(110) Surface: A DFT Study. *Phys. Chem. Chem. Phys.* **2014**, *16*, 12488–12494. [CrossRef]
18. Hong, S.N.; Kye, Y.H.; Yu, C.J.; Jong, U.G.; Ri, G.C.; Choe, C.S.; Kim, K.H.; Han, J.M. Ab Initio Thermodynamic Study of the SnO_2 (110) Surface in an O_2 and NO Environment: A Fundamental Understanding of the Gas Sensing Mechanism for NO and NO_2. *Phys. Chem. Chem. Phys.* **2016**, *18*, 31566–31578. [CrossRef] [PubMed]
19. Vorokhta, M.; Khalakhan, I.; Vondráček, M.; Tomeček, D.; Vorokhta, M.; Marešová, E.; Nováková, J.; Vlček, J.; Fitl, P.; Novotný, M.; et al. Investigation of Gas Sensing Mechanism of SnO_2 Based Chemiresistor Using near Ambient Pressure XPS. *Surf. Sci.* **2018**, *677*, 284–290. [CrossRef]
20. Bolzan, A.A.; Fong, C.; Kennedy, B.J.; Howard, C.J. Structural Studies of Rutile-Type Metal Dioxides. *Acta Crystallogr. Sect. B Struct. Sci.* **1997**, *53*, 373–380. [CrossRef]
21. Fröhlich, D.; Kenklies, R.; Helbig, R. Band-Gap Assignment in SnO_2 by Two-Photon Spectroscopy. *Phys. Rev. Lett.* **1978**, *41*, 1750–1751. [CrossRef]
22. D'Arienzo, M.; Cristofori, D.; Scotti, R.; Morazzoni, F. New Insights into the SnO_2 Sensing Mechanism Based on the Properties of Shape Controlled Tin Oxide Nanoparticles. *Chem. Mater.* **2013**, *25*, 3675–3686. [CrossRef]
23. Buckeridge, J.; Catlow, C.R.A.; Farrow, M.R.; Logsdail, A.J.; Scanlon, D.O.; Keal, T.W.; Sherwood, P.; Woodley, S.M.; Sokol, A.A.; Walsh, A. Deep vs Shallow Nature of Oxygen Vacancies and Consequent N-Type Carrier Concentrations in Transparent Conducting Oxides. *Phys. Rev. Mater.* **2018**, *2*, 56–59. [CrossRef]
24. De Frésart, E.; Darville, J.; Gilles, J.M. Influence of the Surface Reconstruction on the Work Function and Surface Conductance of (110) SnO_2. *Appl. Surf. Sci.* **1982**, *11–12*, 637–651. [CrossRef]
25. Kamp, B.; Merkle, R.; Lauck, R.; Maier, J. Chemical Diffusion of Oxygen in Tin Dioxide: Effects of Dopants and Oxygen Partial Pressure. *J. Solid State Chem.* **2005**, *178*, 3027–3039. [CrossRef]

26. Batzill, M.; Katsiev, K.; Burst, J.M.; Diebold, U.; Chaka, A.M.; Delley, B. Gas-Phase-Dependent Properties of SnO_2 (110), (100), and (101) Single-Crystal Surfaces: Structure, Composition, and Electronic Properties. *Phys. Rev. B-Condens. Matter Mater. Phys.* **2005**, *72*, 1–20. [CrossRef]
27. Yamaguchi, Y.; Nagasawa, Y.; Shimomura, S.; Tabata, K.; Suzuki, E. A Density Functional Theory Study of the Interaction of Oxygen with a Reduced SnO_2 (110) Surface. *Chem. Phys. Lett.* **2000**, *316*, 477–482. [CrossRef]
28. Wang, X.; Qin, H.; Chen, Y.; Hu, J. Sensing Mechanism of SnO_2 (110) Surface to CO: Density Functional Theory Calculations. *J. Phys. Chem. C* **2014**, *118*, 28548–28561. [CrossRef]
29. Eslamian, M.; Salehi, A.; Nadimi, E. The Role of Oxygen Vacancies on SnO_2 Surface in Reducing Cross-Sensitivity between Ambient Humidity and CO: A First Principles Investigation. *Surf. Sci.* **2021**, *708*, 121817. [CrossRef]
30. Xu, G.; Zhang, L.; He, C.; Ma, D.; Lu, Z. Adsorption and Oxidation of NO on Various SnO_2(1 1 0) Surfaces: A Density Functional Theory Study. *Sens. Actuators B Chem.* **2015**, *221*, 717–722. [CrossRef]
31. Prades, J.D.; Cirera, A.; Morante, J.R.; Pruneda, J.M.; Ordejón, P. Ab Initio Study of NOx Compounds Adsorption on SnO_2 Surface. *Sens. Actuators B Chem.* **2007**, *126*, 62–67. [CrossRef]
32. Ducéré, J.-M.; Hemeryck, A.; Estève, A.; Rouhani, M.D.; Landa, G.; Ménini, P.; Tropis, C.; Maisonnat, A.; Fau, P.; Chaudret, B. A Computational Chemist Approach to Gas Sensors: Modeling the Response of SnO_2 to CO, O_2, and H_2O Gases. *J. Comput. Chem.* **2012**, *33*, 247–258. [CrossRef] [PubMed]
33. Abokifa, A.A.; Haddad, K.; Fortner, J.; Lo, C.S.; Biswas, P. Sensing Mechanism of Ethanol and Acetone at Room Temperature by SnO_2 Nano-Columns Synthesized by Aerosol Routes: Theoretical Calculations Compared to Experimental Results. *J. Mater. Chem. A* **2018**, *6*, 2053–2066. [CrossRef]
34. Oviedo, J.; Gillan, M.J. Energetics and Structure of Stoichiometric SnO_2 Surfaces Studied by First-Principles Calculations. *Surf. Sci.* **2000**, *463*, 93–101. [CrossRef]
35. Momma, K.; Izumi, F. VESTA 3 for Three-Dimensional Visualization of Crystal, Volumetric and Morphology Data. *J. Appl. Crystallogr.* **2011**, *44*, 1272–1276. [CrossRef]
36. Yamaguchi, Y.; Nagasawa, Y.; Murakami, A.; Tabata, K. Stability of Oxygen Anions and Hydrogen Abstraction from Methane on Reduced SnO_2 (110) Surface. *Int. J. Quantum Chem.* **1998**, *69*, 669–678. [CrossRef]
37. Cox, D.F.; Fryberger, T.B.; Semancik, S. Oxygen Vacancies and Defect Electronic States on the SnO_2 (110)-1 × 1 Surface. *Phys. Rev. B* **1988**, *38*, 2072–2083. [CrossRef]
38. Sopiha, K.V.; Malyi, O.I.; Persson, C.; Wu, P. Chemistry of Oxygen Ionosorption on SnO_2 Surfaces. *ACS Appl. Mater. Interfaces* **2021**, *13*, 33664–33676. [CrossRef]
39. Trani, F.; Causà, M.; Ninno, D.; Cantele, G.; Barone, V. Density Functional Study of Oxygen Vacancies at the SnO_2 Surface and Subsurface Sites. *Phys. Rev. B-Condens. Matter Mater. Phys.* **2008**, *77*, 2–9. [CrossRef]
40. Guo, Y.; Liang, J.; Liu, Y.; Liu, Y.; Xu, X.; Fang, X.; Zhong, W.; Wang, X. Identifying Surface Active Sites of SnO_2: Roles of Surface O_2^-, O_2^{2-} Anions and Acidic Species Played for Toluene Deep Oxidation. *Ind. Eng. Chem. Res.* **2019**, *58*, 18569–18581. [CrossRef]
41. Simion, C.E.; Schipani, F.; Papadogianni, A.; Stanoiu, A.; Budde, M.; Oprea, A.; Weimar, U.; Bierwagen, O.; Barsan, N. Conductance Model for Single-Crystalline/Compact Metal Oxide Gas-Sensing Layers in the Nondegenerate Limit: Example of Epitaxial SnO_2 (101). *ACS Sens.* **2019**, *4*, 2420–2428. [CrossRef]
42. Chang, S. Oxygen Chemisorption on Tin Oxide: Correlation between Electrical Conductivity and EPR Measurements. *J. Vac. Sci. Technol.* **1980**, *17*, 366–369. [CrossRef]
43. Che, M.; Tench, A.J. Characterization and Reactivity of Mononuclear Oxygen Species on Oxide Surfaces. *Adv. Catal.* **1982**, *31*, 77–133. [CrossRef]
44. Coronado, J.M.; Maira, A.J.; Conesa, J.C.; Yeung, K.L.; Augugliaro, V.; Soria, J. EPR Study of the Surface Characteristics of Nanostructured TiO_2 under UV Irradiation. *Langmuir* **2001**, *17*, 5368–5374. [CrossRef]
45. Coronado, J.M.; Soria, J. ESR Study of the Initial Stages of the Photocatalytic Oxidation of Toluene over TiO_2 Powders. *Catal. Today* **2007**, *123*, 37–41. [CrossRef]
46. Armelao, L.; Barreca, D.; Bontempi, E.; Canevali, C.; Depero, L.E.; Mari, C.M.; Ruffo, R.; Scotti, R.; Tondello, E.; Morazzoni, F. Can Electron Paramagnetic Resonance Measurements Predict the Electrical Sensitivity of SnO_2-Based Film? *Appl. Magn. Reson.* **2002**, *22*, 89–100. [CrossRef]
47. Grishina, D.A.; Mironov, A.A.; Pentegov, I.S.; Marikutsa, A.V.; Konstantinova, E.A. Electron Spin Resonance Characterization of Defects in Sensor Materials Based on Nanocrystalline Tin Dioxide. *Opt. Micro-Nanometrol. IV* **2012**, *8430*, 84300A. [CrossRef]
48. Che, M.; Tench, A.J. Characterization and Reactivity of Molecular Oxygen Species on Oxide Surfaces. *Adv. Catal.* **1983**, *32*, 1–148. [CrossRef]
49. Volodin, A.M.; Cherkashin, A.E. ESR Spectra of O_2^- on SnO_2. Effect of Adsorbed CO on the Conditions of Stabilization of O_2^-. *React. Kinet. Catal. Lett.* **1981**, *17*, 323–327. [CrossRef]
50. Yamazoe, N.; Fuchigami, J.; Kishikawa, M.; Seiyama, T. Interactions of Tin Oxide Surface with O_2, H_2O and H_2. *Surf. Sci.* **1979**, *86*, 335–344. [CrossRef]
51. Matsuura, Y.; Takahata, K.; Ihokura, K. Mechanism of Gas Sensitivity Change with Time of SnO_2 Gas Sensors. *Sens. Actuators* **1988**, *14*, 223–232. [CrossRef]
52. Matsuura, Y.; Takahata, K.; Matsuura, S. Temperature Programmed Desorption Study on Mechanism of Long-Term Deterioration of SnO_2 Gas Sensor. *Denki Kagaku Oyobi Kogyo Butsuri Kagaku* **1990**, *58*, 1154–1161. [CrossRef]

53. Cavicchi, R.; Tarlov, M.; Semancik, S. Preparation of Well-ordered, Oxygen-rich SnO_2 (110) Surfaces via Oxygen Plasma Treatment. *J. Vac. Sci. Technol. A Vac. Surf. Film.* **1990**, *8*, 2347–2352. [CrossRef]
54. Saukko, S.; Lassi, U.; Lantto, V.; Kroneld, M.; Novikov, S.; Kuivalainen, P.; Rantala, T.T.; Mizsei, J. Experimental Studies of O_2-SnO_2 Surface Interaction Using Powder, Thick Films and Monocrystalline Thin Films. *Thin Solid Film.* **2005**, *490*, 48–53. [CrossRef]
55. Capone, S.; Siciliano, P.; Quaranta, F.; Rella, R.; Epifani, M.; Vasanelli, L. Moisture Influence and Geometry Effect of Au and Pt Electrodes on CO Sensing Response of SnO_2 Microsensors Based on Sol-Gel Thin Film. *Sens. Actuators B Chem.* **2001**, *77*, 503–511. [CrossRef]
56. Hahn, S.H.; Bârsan, N.; Weimar, U.; Ejakov, S.G.; Visser, J.H.; Soltis, R.E. CO Sensing with SnO_2thick Film Sensors: Role of Oxygen and Water Vapour. *Thin Solid Film.* **2003**, *436*, 17–24. [CrossRef]
57. Umar, A.; Ammar, H.Y.; Kumar, R.; Almas, T.; Ibrahim, A.A.; AlAssiri, M.S.; Abaker, M.; Baskoutas, S. Efficient H2 Gas Sensor Based on 2D SnO_2 Disks: Experimental and Theoretical Studies. *Int. J. Hydrog. Energy* **2020**, *45*, 26388–26401. [CrossRef]
58. Suematsu, K.; Watanabe, K.; Yuasa, M.; Kida, T.; Shimanoe, K. Effect of Ambient Oxygen Partial Pressure on the Hydrogen Response of SnO_2 Semiconductor Gas Sensors. *J. Electrochem. Soc.* **2019**, *166*, B618–B622. [CrossRef]
59. Grossmann, K.; Pavelko, R.G.; Barsan, N.; Weimar, U. Interplay of H_2, Water Vapor and Oxygen at the Surface of SnO_2 Based Gas Sensors—An Operando Investigation Utilizing Deuterated Gases. *Sens. Actuators B Chem.* **2012**, *166–167*, 787–793. [CrossRef]
60. Hübner, M.; Pavelko, R.G.; Barsan, N.; Weimar, U. Influence of Oxygen Backgrounds on Hydrogen Sensing with SnO_2 Nanomaterials. *Sens. Actuators B Chem.* **2011**, *154*, 264–269. [CrossRef]
61. Choi, P.G.; Izu, N.; Shirahata, N.; Masuda, Y. SnO_2 Nanosheets for Selective Alkene Gas Sensing. *ACS Appl. Nano Mater.* **2019**, *2*, 1820–1827. [CrossRef]
62. Kooti, M.; Keshtkar, S.; Askarieh, M.; Rashidi, A. Progress toward a Novel Methane Gas Sensor Based on SnO_2 Nanorods-Nanoporous Graphene Hybrid. *Sens. Actuators B Chem.* **2019**, *281*, 96–106. [CrossRef]
63. Chen, Y.; Wang, X.; Shi, C.; Li, L.; Qin, H.; Hu, J. Sensing Mechanism of SnO_2 (1 1 0) Surface to H_2: Density Functional Theory Calculations. *Sens. Actuators B Chem.* **2015**, *220*, 279–287. [CrossRef]
64. Barsan, N.; Rebholz, J.; Weimar, U. Conduction Mechanism Switch for SnO_2 Based Sensors during Operation in Application Relevant Conditions; Implications for Modeling of Sensing. *Sens. Actuators B Chem.* **2015**, *207*, 455–459. [CrossRef]
65. Santarossa, G.; Hahn, K.; Baiker, A. Free Energy and Electronic Properties of Water Adsorption on the SnO_2 (110) Surface. *Langmuir* **2013**, *29*, 5487–5499. [CrossRef]
66. Leblanc, E.; Perier-Camby, L.; Thomas, G.; Gibert, R.; Primet, M.; Gelin, P. NOx Adsorption onto Dehydroxylated or Hydroxylated Tin Dioxide Surface. Application to SnO_2-Based Sensors. *Sens. Actuators B Chem.* **2000**, *62*, 67–72. [CrossRef]
67. Wicker, S.; Guiltat, M.; Weimar, U.; Hémeryck, A.; Barsan, N. Ambient Humidity Influence on CO Detection with SnO_2 Gas Sensing Materials. A Combined DRIFTS/DFT Investigation. *J. Phys. Chem. C* **2017**, *121*, 25064–25073. [CrossRef]
68. Thoren, W.; Kohl, D.; Heiland, G. Kinetic Studies of the Decomposition of CH_3COOH and CH_3COOD on SnO_2 Single Crystals. *Surf. Sci.* **1985**, *162*, 402–410. [CrossRef]
69. Tamaki, J.; Nagaishi, M.; Teraoka, Y.; Miura, N.; Yamazoe, N.; Moriya, K.; Nakamura, Y. Adsorption Behavior of CO and Interfering Gases on SnO_2. *Surf. Sci.* **1989**, *221*, 183–196. [CrossRef]
70. Wang, D.; Chen, Y.; Liu, Z.; Li, L.; Shi, C.; Qin, H.; Hu, J. CO_2-Sensing Properties and Mechanism of Nano-SnO_2 Thick-Film Sensor. *Sens. Actuators B Chem.* **2016**, *227*, 73–84. [CrossRef]
71. Kim, D.H.; Yoon, J.Y.; Park, H.C.; Kim, K.H. CO_2-Sensing Characteristics of SnO_2 Thick Film by Coating Lanthanum Oxide. *Sens. Actuators B Chem.* **2000**, *62*, 61–66. [CrossRef]
72. Hsu, K.C.; Fang, T.H.; Hsiao, Y.J.; Chan, C.A. Highly Response CO_2 Gas Sensor Based on Au-La_2O_3 Doped SnO_2 Nanofibers. *Mater. Lett.* **2020**, *261*, 127144. [CrossRef]
73. Kim, H.Y.; Lee, H.M.; Pala, R.G.S.; Shapovalov, V.; Metiu, H. CO Oxidation by Rutile TiO_2 (110) Doped with V, W, Cr, Mo, and Mn. *J. Phys. Chem. C* **2008**, *112*, 12398–12408. [CrossRef]
74. Ramesh, K.; Chen, L.; Chen, F.; Liu, Y.; Wang, Z.; Han, Y.F. Re-Investigating the CO Oxidation Mechanism over Unsupported MnO, Mn_2O_3 and MnO_2 Catalysts. *Catal. Today* **2008**, *131*, 477–482. [CrossRef]
75. Zakaryan, H.A.; Aroutiounian, V.M. Ab Initio Investigation of CO Gas Sensing Mechanism on SnO_2 Surfaces. *Allsensor* **2017**, *27*, 50–55.
76. Degler, D.; Wicker, S.; Weimar, U.; Barsan, N. Identifying the Active Oxygen Species in SnO_2 Based Gas Sensing Materials: An Operando IR Spectrsocopy Study. *J. Phys. Chem. C* **2015**, *119*, 11792–11799. [CrossRef]
77. Degler, D.; Barz, N.; Dettinger, U.; Peisert, H.; Chassé, T.; Weimar, U.; Barsan, N. Extending the Toolbox for Gas Sensor Research: Operando UV/Vis Diffuse Reflectance Spectroscopy on SnO_2-Based Gas Sensors. *Sens. Actuators B Chem.* **2016**, *224*, 256–259. [CrossRef]
78. Ruhland, B.; Becker, T.; Müller, G. Gas-Kinetic Interactions of Nitrous Oxides with SnO_2surfaces. *Sens. Actuators B Chem.* **1998**, *50*, 85–94. [CrossRef]
79. Sergent, N.; Epifani, M.; Pagnier, T. In Situ Raman Spectroscopy Study of NO_2 Adsorption onto Nanocrystalline Tin (IV) Oxide. *J. Raman Spectrosc.* **2006**, *37*, 1272–1277. [CrossRef]
80. Maeng, S.; Kim, S.W.; Lee, D.H.; Moon, S.E.; Kim, K.C.; Maiti, A. SnO_2 Nanoslab as NO_2 Sensor: Identification of the NO_2 Sensing Mechanism on a SnO_2 Surface. *ACS Appl. Mater. Interfaces* **2014**, *6*, 357–363. [CrossRef] [PubMed]

81. Maiti, A.; Rodriguez, J.A.; Law, M.; Kung, P.; McKinney, J.R.; Yang, P. SnO_2 Nanoribbons as NO_2 Sensors: Insights from First Principles Calculations. *Nano Lett.* **2003**, *3*, 1025–1028. [CrossRef]
82. Epifani, M.; Prades, J.D.; Comini, E.; Pellicer, E.; Avella, M.; Faglia, G.; Cirera, A.; Scotti, R.; Morazzoni, F.; Morante, J.R. The Role of Surface Oxygen Vacancies in the NO_2 Sensing Properties of SnO_2 Nanocrystals. *J. Phys. Chem. C* **2008**, *112*, 19540–19546. [CrossRef]
83. Wei, Y.; Chen, C.; Yuan, G.; Gao, S. SnO_2nanocrystals with Abundant Oxygen Vacancies: Preparation and Room Temperature NO_2sensing. *J. Alloys Compd.* **2016**, *681*, 43–49. [CrossRef]
84. Zhong, Y.; Li, W.; Zhao, X.; Jiang, X.; Lin, S.; Zhen, Z.; Chen, W.; Xie, D.; Zhu, H. High-Response Room-Temperature NO_2 Sensor and Ultrafast Humidity Sensor Based on SnO_2 with Rich Oxygen Vacancy. *ACS Appl. Mater. Interfaces* **2019**, *11*, 13441–13449. [CrossRef] [PubMed]
85. Prades, J.D.; Cirera, A.; Morante, J.R. First-Principles Study of NOx and SO_2 Adsorption onto SnO_2 (110). *J. Electrochem. Soc.* **2007**, *154*, H675. [CrossRef]
86. Watkins, G.D. Negative-U Properties for Defects in Solids. In *Advances in Solid State Physics*; Springer: Berlin/Heidelberg, Germany, 1984; Volume 24, pp. 163–189. [CrossRef]
87. Lany, S.; Zakutayev, A.; Mason, T.O.; Wager, J.F.; Poeppelmeier, K.R.; Perkins, J.D.; Berry, J.J.; Ginley, D.S.; Zunger, A. Surface Origin of High Conductivities in Undoped In_2O_3 Thin Films. *Phys. Rev. Lett.* **2012**, *108*, 2–6. [CrossRef]